Available online at www.sciencedirect.com
ScienceDirect
Trans. Nonferrous Met. Soc. China 32(2022) 838−849
Transactions of Nonferrous Metals Society of China
www.tnmsc.cn

Effects of Li content on microstructure and mechanical properties of as-cast Mg−*x*Li−3Al−2Zn−0.5Y alloys

Xiang PENG, Wen-cai LIU, Guo-hua WU

National Engineering Research Center of Light Alloy Net Forming and State Key Laboratory of Metal Matrix Composite, School of Materials Science and Engineering, Shanghai Jiao Tong University, Shanghai 200240, China

Received 8 October 2021; accepted 10 January 2022

Abstract: The effects of Li content on the microstructure and mechanical properties of the as-cast Mg−*x*Li−3Al−2Zn−0.5Y (LAZ*x*32-0.5Y) alloys were investigated by XRD, SEM, TEM, hardness tester and universal testing machine. The results show that the matrix of the alloy transforms from α-Mg to α-Mg+β-Li and then to β-Li when the Li content increases from 4% to 14% (mass fraction). All LAZ*x*32-0.5Y alloys contain AlLi and Al_2Y, while $MgLi_2Al$ appears only in the alloy containing the β-Li matrix. As the Li content increases, the content of AlLi and $MgLi_2Al$ gradually increases, while the content of Al_2Y does not change much. As the Li content increases from 4% to 10%, the ultimate tensile strength and hardness of the as-cast LAZ*x*32-0.5Y alloys gradually decrease while the elongation gradually increases. The corresponding fracture mechanism changes from cleavage fracture to quasi-cleavage fracture and then to microporous aggregation fracture. This is mainly attributed to the decrease of α-Mg and the increase of β-Li in the alloy. When the Li content continues to increase to 10% and 14%, the yield strength, ultimate tensile strength and hardness of the as-cast LAZ*x*32-0.5Y alloys gradually increase, while the elongation decreases sharply, which is mainly attributed to the nano-scale $MgLi_2Al$ uniformly distributed in the β-Li matrix.

Key words: Mg−Li alloy; li content; alloying; microstructure; mechanical properties

1 Introduction

Mg−Li alloy, as the world's lightest metal structural material, has been favored in many fields such as aerospace, military, and electronics due to its low density and good plastic deformation ability [1]. However, low strength severely restricts the in-depth research and wide application of Mg−Li alloy.

Alloying is one of the simplest and most effective ways to improve the strength of Mg−Li alloy. Al and Zn are the most commonly used alloying elements to improve the strength of Mg−Li alloy through solid solution strengthening and second phase strengthening [2]. It has been shown that the strength of Mg−Li alloy gradually increases with increasing Al content. However, when the Al content is larger than 5%−6%, as the Al content continues to increase, the strength of the alloy does not increase significantly, while the elongation decreases substantially [3]. The strengthening effect of Zn is similar to that of Al, but less than that of Al. In addition, the addition of Zn increases the density and weakens the corrosion resistance of the Mg−Li alloy when the content of Zn in the Mg alloy is larger than 2.5%. Therefore, the content of Mg is usually controlled to 2% [4]. In general, Al and Zn are usually added together to Mg−Li alloy to take the full advantages of their respective properties. The rare earth elements are also commonly used as alloying elements due to their effect of refining the alloy grains, purifying the alloy melt, and improving the mechanical properties of the alloy.

Corresponding author: Wen-cai LIU, Tel: +86-21-54742630, Fax: +86-21-34202794, E-mail: liuwc@sjtu.edu.cn
DOI: 10.1016/S1003-6326(22)65837-0

Among them, Y has the same hcp structure as Mg and has a high solid solubility (3.5%, mole fraction) in Mg, which can enhance the strength of the Mg−Li alloy through solid solution strengthening [5]. The density of Y is 4.469 g/cm^3, and it does not lead to a significant increase in the density of the Mg−Li alloy. In addition, Y can also form Al_2Y strengthening phase, which improves the mechanical properties of the alloy through the second phase strengthening. At present, a large number of studies have been reported on Mg−Li−Al−Zn−Y alloys due to their good mechanical properties [6−11], but there are few reports on the microstructure and properties of Mg−Li−Al−Zn−Y alloys with different Li contents.

In this work, the effects of different Li contents on the microstructure and mechanical properties of as-cast Mg−*x*Li−3Al−2Zn−0.5Y (LAZ*x*32-0.5Y) alloys are investigated. The microstructure evolution with Li content and strengthening mechanism of the alloy are discussed.

2 Experimental

The LAZ*x*32-0.5Y alloys were prepared in a vacuum induction melting furnace under argon protection. The raw materials were made of pure Li (>99.9%) pure Mg (>99.9%), pure Al (>99.9%), pure Zn (>99.9%) and Mg−20%Y master alloy. The chemical composition of the alloy was determined by inductively coupled plasma optical emission spectroscopy (ICP-AES, Perkin Elmer Plasma−400). The density of the alloy samples was measured by an electronic balance (AEL−200). The phase analysis was carried out by X-ray diffraction (XRD, D8 ADVANCE Da Vinci) using a Rigaku D/max instrument with a scan step of 5 (°)/min. The microstructure and fracture morphology were observed by scanning electron microscope (SEM, Phenom XL) equipped with an energy dispersive spectrometer (EDS), electron probe (EPMA) and transmission electron microscope (TEM, JEOL 2100F and JEOL 2100). The hardness was measured with a Vickers hardness tester (XHVT−10Z). The tensile specimens with a diameter of 6 mm and a length of 30 mm in the gauge section were cut from the samples according to GB/T 228.1—2010 standards. The tensile tests were carried out on a testing machine (Zwick/Roell Z020) with a fixed strain rate of 2 mm/min at room temperature. Five specimens were tested for each condition to ensure the repeatability of the experiments.

3 Results

3.1 Microstructure

Table 1 lists the actual chemical composition and density of the LAZ*x*32-0.5Y alloys. According to Table 1, the actual chemical compositions of the alloys are close to the nominal composition, which can reflect the microstructure and properties of the designed alloys. With the increase of Li content, the density of the LAZ*x*32-0.5Y alloys gradually decreases. When the Li content increases from 4% to 14%, the density of the alloy gradually decreases from 1.674 g/cm^3 to 1.411 g/cm^3. Lithium, the lightest metallic element, has a density of only 0.534 g/cm^3. Therefore, the density of the alloy gradually decreases with increasing Li content. It has been shown that the density of binary Mg−Li alloy can be estimated and predicted by the equation ρ=1.74−2.46x (ρ is the density and x is the mass fraction of Li) [12]. When the Li contents are 4%, 6%, 8%, 10%, 12%, and 14%, the estimated densities of the corresponding binary Mg−Li alloys

Table 1 Chemical composition and density of tested alloys

Nominal composition	Density/ (g·cm^{-3})	Actual composition (mass fraction)/%				
		Li	Al	Zn	Y	Mg
Mg−4Li−3Al−2Zn−0.5Y	1.674	4.16	3.03	1.79	0.27	Bal.
Mg−6Li−3Al−2Zn−0.5Y	1.587	6.42	2.96	2.02	0.27	Bal.
Mg−8Li−3Al−2Zn−0.5Y	1.541	8.30	2.79	2.08	0.28	Bal.
Mg−10Li−3Al−2Zn−0.5Y	1.496	10.20	2.90	1.86	0.30	Bal.
Mg−12Li−3Al−2Zn−0.5Y	1.460	11.97	3.06	1.84	0.28	Bal.
Mg−14Li−3Al−2Zn−0.5Y	1.411	14.18	2.76	1.88	0.27	Bal.

are 1.642, 1.593, 1.543, 1.494, 1.445 and 1.396 g/cm^3, respectively. Since some Al, Zn and Y are also added to the LAZ*x*32-0.5Y alloys, the actual density of the alloys should be slightly larger than the estimated density. The actual densities of the as-cast LAZ632-0.5Y and LAZ832-0.5Y alloys are slightly lower than the estimated densities, mainly due to the actual Li contents of 6.42% (>6%) and 8.30% (>8%), respectively.

The XRD patterns of the as-cast LAZ*x*32-0.5Y alloys are shown in Fig. 1. It can be seen that the matrix phase of the as-cast LAZ432-0.5Y alloy is *α*-Mg (solid solution formed by Li solid dissolved in Mg), which is a typical *α*-Mg single phase alloy. When the Li content increases to 6% and 8%, the matrix phases of both LAZ632-0.5Y and LAZ832-0.5Y alloys contain *α*-Mg and *β*-Li (solid solution formed by Mg solid dissolved in Li), which are typical *α*-Mg+*β*-Li double phase alloys. When the Li content increases to 10%, the matrix phase of the LAZ1032-0.5Y alloy is dominated by *β*-Li, and only a few *α*-Mg diffraction peaks can be observed in the XRD patterns. When the Li content continues to increase to 12% and 14%, the matrix phases of the LAZ1232-0.5Y and LAZ1432-0.5Y alloys are completely transformed to *β*-Li, which is a typical *β*-Li single phase alloy. With the increase of Li content from 4% to 14%, the matrix phase of the as-cast LAZ*x*32-0.5Y alloys transforms from *α*-Mg single phase to *α*-Mg+*β*-Li double phase and then to *β*-Li single phase, which coincides with the phase diagram of the Mg−Li binary alloy [12]. The addition of Al, Zn and Y elements leads to the formation of the second phase in the LAZ*x*32-0.5Y alloys. All the LAZ*x*32-0.5Y alloys contain AlLi phase and Al_2Y phase. The content of AlLi phase gradually increases with the increase of Li content, but when the Li content increases to 14%, the increase of AlLi phase is not obvious. The diffraction peaks of $MgLi_2Al$ phase are detected in all the alloys except LAZ432-0.5Y alloy, and the $MgLi_2Al$ content gradually increases with the increase of Li content. What's more, the diffraction peaks of the second phase containing Zn do not appear in the XRD patterns, indicating that Zn is mainly solid dissolved in the Mg matrix.

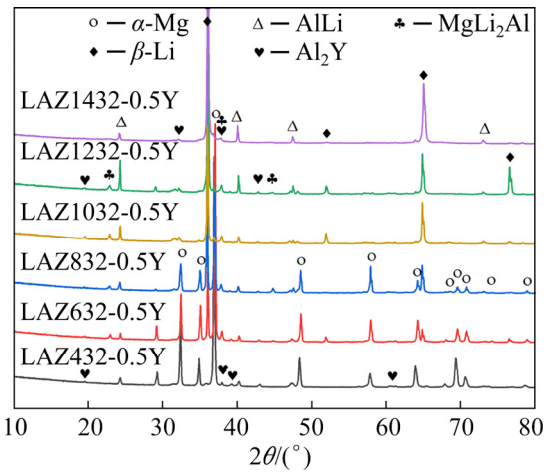

Fig. 1 XRD patterns of as-cast Mg−*x*Li−3Al−2Zn−0.5Y (*x*=4, 6, 8, 10, 12 and 14) alloys

The microstructures of the as-cast LAZ*x*32-0.5Y alloys are shown in Fig. 2. As can be seen from Figs. 2(a, a_1), the as-cast LAZ432-0.5Y alloys have a light gray *α*-Mg matrix phase, with fine white massive phases distributed in the *α*-Mg matrix. There is a continuous eutectic reticular tissue along the grain boundaries. It has been reported that the reticular tissue is formed by alternating layers of filamentous AlLi phase and *α*-Mg phase [13]. The EDS analysis shows that the fine massive phase in the alloys mainly contains Al (67.40%, mole fraction) and Y (32.6%, mole fraction), and the Al/Y mole ratio is close to 2:1. Combined with the XRD results in Fig. 1, it can be known that this white massive phase is Al_2Y. As can be seen from Figs. 2(b, b_1, c, c_1), the as-cast LAZ632-0.5Y and LAZ832-0.5Y alloys are typical double phase alloys, with the light gray matrix phase being the *α*-Mg and the dark gray matrix phase being the *β*-Li. When the Li content increases from 6% to 8%, the *α*-Mg in the alloy decreases and changes from coarse massive to long strip or small massive; while the content of *β*-Li increases substantially. The EDS results show that the Al/Y mole ratio in the bright white massive phase is close to 2:1, which is identified as Al_2Y. In addition, white granular phase can be observed in the *β*-Li matrix and distributed along the *α*-Mg/*β*-Li phase interface, which is weaker in brightness than the Al_2Y. It has been shown that the AlLi phase has different forms in *α*-Mg and *β*-Li, i.e., it is present in *α*-Mg in filamentous form, while it is present in *β*-Li in granular form [14,15]. Combined with the relevant literature, it can be assumed that the larger granular phase with slightly darker contrast is AlLi phase. In addition to the larger granular AlLi phase, nano-scale particles can be observed in the *β*-Li matrix, and these particles are either present

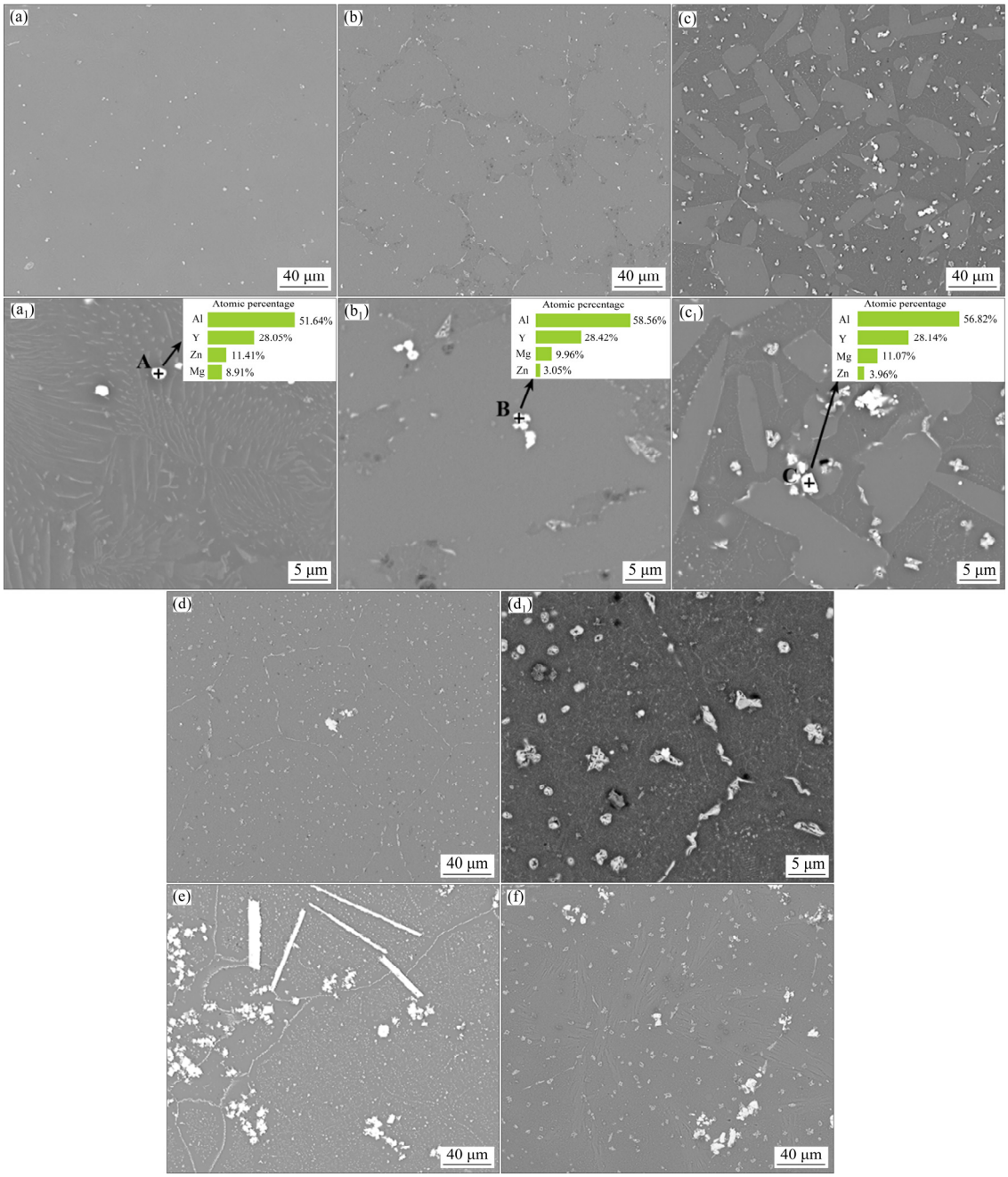

Fig. 2 SEM images of as-cast LAZ*x*32-0.5Y alloys: (a, a_1) *x*=4; (b, b_1) *x*=6; (c, c_1) *x*=8; (d, d_1) *x*=10; (e) *x*=12; (f) *x*=14

individually as particles or in series as fine lines. Based on the XRD results and the related literature, these nano-scale particles could be the $MgLi_2Al$ [16]. It can be seen from Figs. 2(d, d_1) that when the Li content increases to 10%, the matrix of the alloy almost completely transforms into the *β*-Li, and the bright white Al_2Y phase, white granular AlLi phase and fine granular phase (probably $MgLi_2Al$ phase) are also distributed in the *β*-Li matrix. It can be seen from Figs. 2(e, f) that the LAZ1232-0.5Y and LAZ1432-0.5Y alloys are *β*-Li single phase alloys and have similar second phase with the LAZ1032-0.5Y alloy. However, the content of AlLi and $MgLi_2Al$ in the alloy increases with the increase of Li content. In addition, massive and long Al_2Y phase is observed in the as-cast LAZ1232-0.5Y alloy, which appears to aggregate in some regions.

The elemental map scanning analysis of the as-cast LAZ1232-0.5Y alloy is shown in Fig. 3. As can be seen, the bright white massive phase in the alloy is mainly enriched in Al and Y, indicating the Al_2Y. The white particles are mainly rich in Al and Zn, and are identified as $MgLi_2Al$ and AlLi.

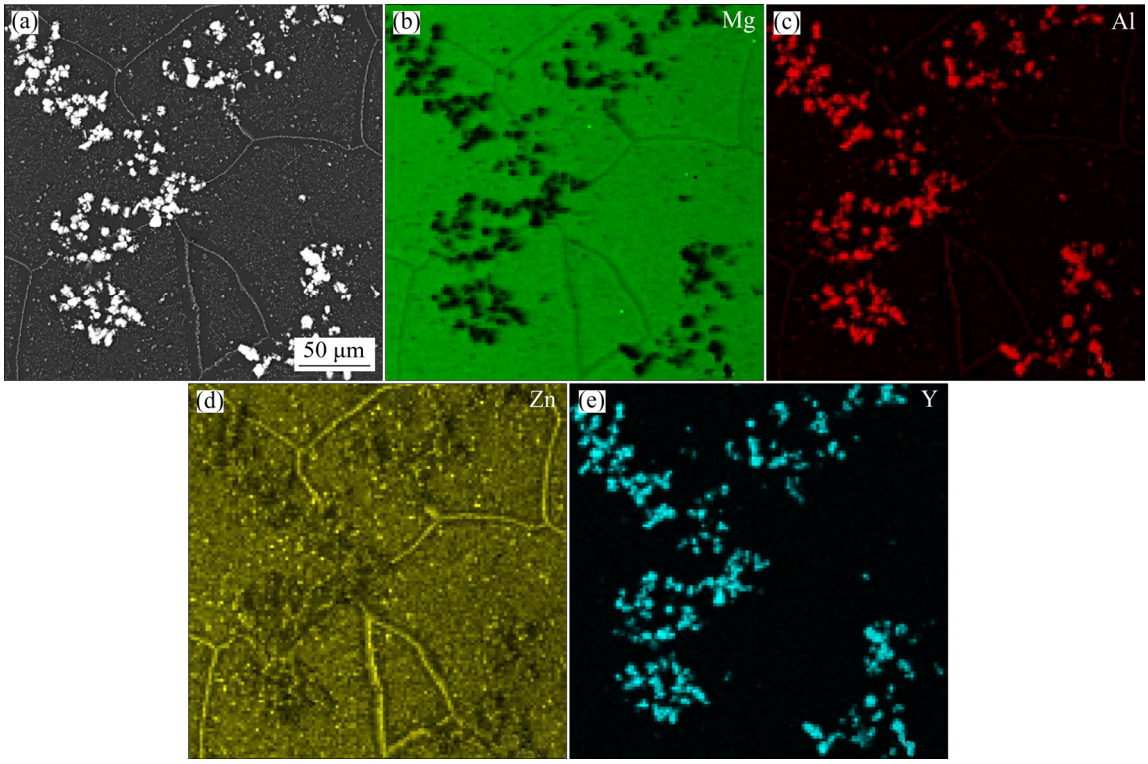

Fig. 3 Map scanning analysis of as-cast Mg−12Li−3Al−2Zn−0.5Y alloy

TEM images of the as-cast LAZ832-0.5Y alloy are shown in Fig. 4. The *α*-Mg/*β*-Li interface can be clearly observed in Fig. 4(a), and the diffraction spot corresponding to the $[2\bar{1}\bar{1}0]$ crystal band axis of the *α*-Mg matrix is given in the upper right corner. The massive *α*-Mg is slightly floating and embedded in the *β*-Li, which is caused by the fact that the *β*-Li is more easily thinned by the ion beam during the preparation of the TEM specimen. Figure 4(b) shows the enlarged *α*-Mg/*β*-Li interface, which is flat and clear. The left region is clean and almost free of the second phase, which is *α*-Mg; and the right region is *β*-Li. Diffraction analysis shows that the polygonal massive second phase is Al_2Y, as seen in Fig. 4(c). In addition, many nano-scale particles are observed in the as-cast LAZ832-0.5Y alloy. Diffraction analysis reveals that these nano-scale particles are face-centered cubic (fcc) structures. Combined with the XRD results in Fig. 1, it is clear that the as-cast LAZ832-0.5Y alloy contains Al_2Y, AlLi and $MgLi_2Al$. Both the AlLi and $MgLi_2Al$ have fcc structures and their lattice parameters are very close, so it is difficult to distinguish them. Since the $MgLi_2Al$ is prone to over aging and transforming into AlLi, leading to coexistence of AlLi and $MgLi_2Al$. Therefore, these nano-scale particles can be referred to as Al−Li.

3.2 Mechanical properties

The Vickers hardness is shown in Fig. 5. It can be seen that when the Li content is 4%, 6%, 8%, 10%, 12% and 14%, the Vickers hardness of the alloys is 62.3, 61.2, 59.6, 56.0, 71.2 and 72.3 HV, respectively. With the increase of Li content, the hardness of the as-cast LAZ*x*32-0.5Y alloy shows a trend of decreasing and then increasing, and reaches the minimum value at 10% Li.

The mechanical properties of the as-cast LAZ*x*32-0.5Y alloys are shown in Fig. 6. When the Li content increases from 4% to 10%, the ultimate tensile strength of the alloys is 184.3, 178.5, 167.8 and 145.0 MPa, the yield strength is 115.3, 130.3, 137.5 and 120.0 MPa, and the elongation is 4.4%, 6.8%, 12.6% and 24.7%, respectively. It can be seen that as the Li content increases, the ultimate tensile strength of the LAZ*x*32-0.5Y alloys gradually decreases and the elongation gradually increases, while the yield strength first increases and then decreases. When the Li content continues to increase to 12% and 14%, the ultimate tensile

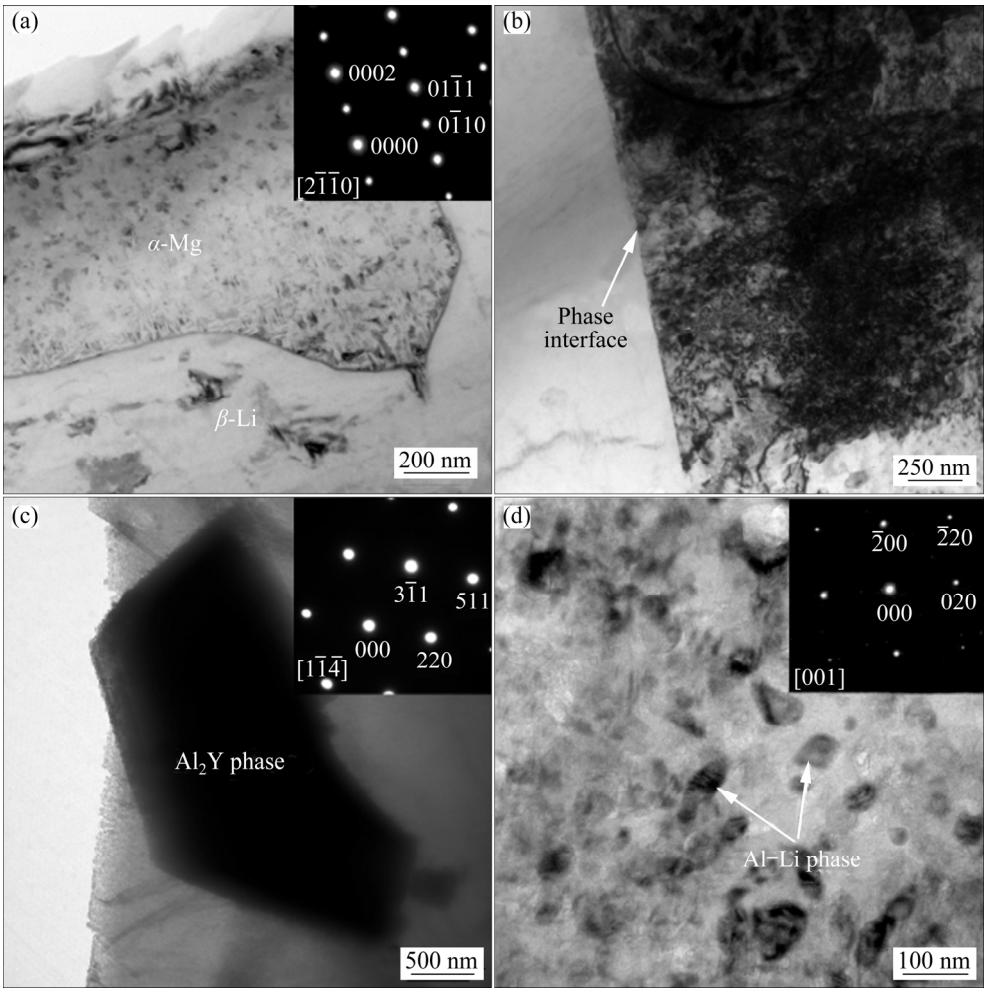

Fig. 4 TEM images of as-cast Mg−8Li−3Al−2Zn−0.5Y alloy

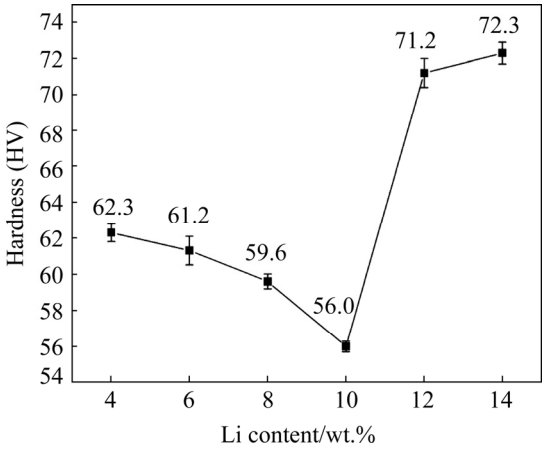

Fig. 5 Hardness of as-cast LAZ*x*32-0.5Y (*x*=4, 6, 8, 10, 12 and 14) alloys

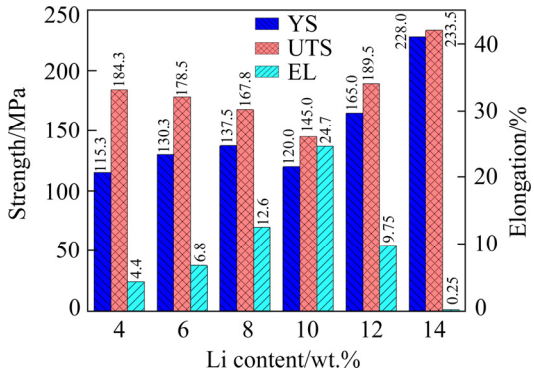

Fig. 6 Mechanical properties of as-cast Mg−*x*Li−3Al−2Zn−0.5Y (*x*=4, 6, 8, 10, 12 and 14) alloys

strength of the alloy is 189.5 and 233.5 MPa, the yield strength is 165.0 and 228.0 MPa, and the elongation is 9.75% and 0.25%, respectively. It can be seen that when the Li content continues to increase above 10%, the ultimate tensile strength and yield strength continually increase, while the elongation decreases substantially. The changing trend of the ultimate tensile strength with Li content remains consistent with that of the hardness in Fig. 5.

Figure 7 shows the fracture morphologies of the as-cast LAZ*x*32-0.5Y alloys. As can be seen, the

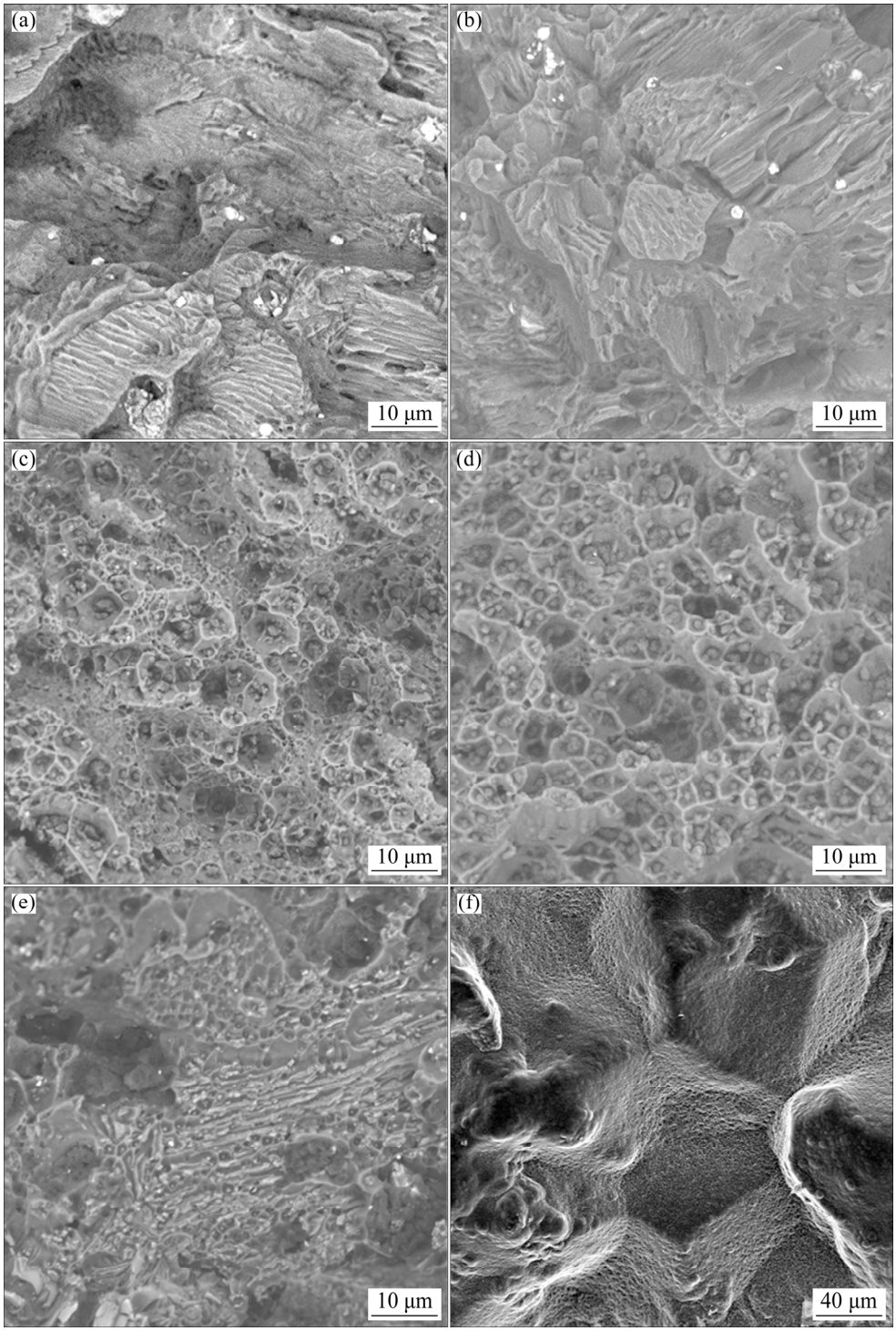

Fig. 7 Fracture surfaces of as-cast LAZ*x*32-0.5Y alloys: (a) *x*=4; (b) *x*=6; (c) *x*=8; (d) *x*=10; (e) *x*=12; (f) *x*=14

fracture surfaces of the LAZ432-0.5Y and LAZ632-0.5Y alloys are covered with cleavage steps, which is a typical cleavage fracture. The fracture surface of the as-cast LAZ832-0.5Y alloy shows many dimples and some tearing ridges, which indicates quasi-cleavage fracture. The fracture surface of the LAZ1032-0.5Y alloy is covered with many dimples, and many second phase particles are observed at the bottom of the dimples, which is typical of ductile fracture. The fracture surface of the LAZ1232-0.5Y alloy is covered with cleavage steps, dimples and tearing ridges, which is a quasi-cleavage fracture. The fracture surface of the LAZ1432-0.5Y alloy is icing sugar-like, and grain boundaries can be clearly observed, which is typical of brittle intergranular

fracture. When the Li content increases from 4% to 10%, the fracture morphology of the LAZ*x*32-0.5Y alloys shows a continuous transformation: cleavage steps → tearing ridges + dimples → dimples. This indicates that the ductility of the alloy increases continuously with the increase of Li content, which is consistent with the elongation results shown in Fig. 6. When the Li content continues to increase to 12% and 14%, the fracture of the alloy changes from dimple fracture to quasi-cleavage and intergranular fracture, indicating that the ductility decreases substantially, which is consistent with the elongation results.

4 Discussion

4.1 Effect of Li content on microstructure of Mg−Li alloy

According to the phase diagram of Mg−Li binary alloy, when the Li content is lower than 5.7%, Mg−Li alloy is *α*-Mg single phase alloy. *α*-Mg phase is the solid solution of Li with a dense hexagonal (hcp) structure. When the Li content is higher than 10.3%, Mg−Li alloy is *β*-Li single-phase alloy. *β*-Li phase is the solid solution of Mg with body-centered cubic (bcc) structure. When the Li content is between 5.7% and 10.3%, Mg−Li alloy is *α*-Mg + *β*-Li double phase alloy [17,18]. Therefore, the LAZ432-0.5Y alloy is a typical *α*-Mg single phase alloy, and obvious *α*-Mg without *β*-Li diffraction peaks can be detected in the corresponding XRD patterns. The actual contents of Li in the LAZ632-0.5Y and LAZ832-0.5Y alloys are 6.42% and 8.30%, respectively, which are typical *α*-Mg+*β*-Li double phase alloys. Obvious *α*-Mg and *β*-Li diffraction peaks are detected simultaneously in the corresponding XRD patterns. The actual content of Li in the LAZ1032-0.5Y alloy is 10.20%, which is very close to 10.3%. Therefore, the matrix of the LAZ1032-0.5Y alloy is dominated by *β*-Li, and only a few small *α*-Mg phases can be observed in the *β*-Li matrix (as shown in Fig. 2(d_1)). In addition, obvious *β*-Li diffraction peaks can be detected in the corresponding XRD patterns. The actual contents of Li in the as-cast LAZ1232-0.5Y and LAZ1432-0.5Y alloys are 11.97% and 14.18%, respectively, which are typical *β*-Li single phase alloys. Obvious *β*-Li without *α*-Mg diffraction peaks can be detected in the corresponding XRD patterns. Obviously, with the increase of Li content, the matrix of the as-cast LAZ*x*32-0.5Y alloys changes from *α*-Mg single phase to *α*-Mg+*β*-Li double phase, and then to *β*-Li single phase. Accordingly, the crystal structure of the as-cast LAZ*x*32-0.5Y alloys changes from hcp to hcp+bcc and then to bcc, which is consistent with the phase diagram of Mg−Li alloy.

In the LAZ*x*32-0.5Y alloys, the addition of Al, Zn and Y leads to the formation of the second phases. The possibility of forming compounds between different elements depends on the electronegativity difference. Generally, the larger the electronegativity difference value, the stronger the bonding between the elements and the easier it is to form intermetallic compounds [19,20]. Table 2 lists the electronegativity and atomic radius of the alloying elements in LAZ*x*32-0.5Y alloys. It can be seen that the electronegativity difference between Al and Li is the largest (64.28%), which is slightly higher than that between Zn and Li. Therefore, when both Al and Zn are added to the Mg−Li alloy, Li preferentially forms intermetallic compounds (AlLi and $MgLi_2Al$) with Al. In addition, the electronegativity difference between Al and Y is 31.96%, which is higher than that between other alloying elements and Y. So Al preferentially combines with the Y to form Al_2Y. Most of the Al form intermetallic compounds (AlLi, $MgLi_2Al$ and Al_2Y) with Li and Y in the alloy, and the remaining part of Al is solid dissolved in the matrix. Since the solid solution of Al in Mg is larger than that of Al in Li, the remaining part of Al is mainly solid dissolved in the *α*-Mg matrix. Combined with the XRD results and the electronegativity difference analysis, it is clear that Zn does not form any intermetallic compounds, but dissolves into the alloy. Zn is mainly solid dissolved in the *β*-Li matrix and second phase containing Al, because the solid solution of Zn in Al and Li is much higher than that of Zn in Mg. Therefore, Zn mainly plays a solid solution strengthening role. Y mainly forms Al_2Y, which enhances the strength of the alloy through the second phase strengthening. Furthermore, it has been shown that the $MgLi_2Al$ phase precipitates from the *β*-Li matrix and then transforms into the stable AlLi phase at room temperature, i.e., *β*-Li → $MgLi_2Al$ → AlLi [21,22]. Thus, the AlLi and Al_2Y phases are detected in all alloys, while $MgLi_2Al$ is detected only in the alloys containing *β*-Li. As the Li content increases, more

Table 2 Electronegativity and atomic radius of elements in LAZ*x*32-0.5Y alloys

Element	Electronegativity	Electronegativity difference with Li/%	Electronegativity difference with Y/%	Atomic radius/Å	Atomic radius difference with Li/%	Atomic radius difference with Y/%
Mg	1.31	33.67	7.37	1.60	3.22	12.08
Li	0.98	0	19.67	1.55	0	14.83
Al	1.61	64.28	31.96	1.43	7.74	21.42
Zn	1.60	63.26	31.14	1.33	14.19	26.92
Y	1.22	24.49	0	1.82	17.42	0

Al combines with Li to form AlLi and $MgLi_2Al$ phases, resulting in less Al solid dissolved in the matrix.

4.2 Effect of Li content on mechanical properties of Mg−Li alloy

When the Li content increases from 4% to 10%, the ultimate tensile strength and hardness of the as-cast LAZ*x*32-0.5Y alloys gradually decrease, the elongation gradually increases, while the yield strength first increases and then decreases. When the Li content continues to increase above 10%, the yield strength, ultimate tensile strength and hardness increase continuously and are higher than those of the LAZ432-0.5Y alloy, while the elongation decreases substantially. The trends in the mechanical properties of the as-cast LAZ*x*32-0.5Y alloys can be explained from various aspects.

(1) Matrix analysis: with the increase of Li content, the matrix of the alloy changes from α-Mg to α-Mg+β-Li and then to β-Li. In the Mg−Li alloy, the α-Mg matrix with hcp structure has higher hardness, higher strength and worse ductility, while the β-Li matrix with bcc structure has lower strength and hardness and better ductility. The matrix of the as-cast LAZ432-0.5Y alloy is α-Mg phase, and has high strength and hardness as well as low elongation. When the Li content increases from 4% to 10%, β-Li matrix appears in the alloy, and the content of β-Li gradually increases until the α-Mg matrix basically disappears. Accordingly, the ultimate tensile strength and hardness of the alloy gradually decrease with the increase of β-Li content, while the elongation gradually increases. Yield strength is the yield limit of a metallic material when yielding occurs, and is also the stress that resists a trace of plastic deformation. The yield strength of the double phase LAZ632-0.5Y and LAZ832-0.5Y alloys is higher than that of the single phase LAZ432-0.5Y and LAZ1032-0.5Y alloys. The reason is that in the double phase Mg−Li alloys, the softer β-Li with more slip systems preferentially undergoes plastic deformation, and the stress is transferred from β-Li to α-Mg. When the stress is larger than the elastic limit of α-Mg, plastic deformation of α-Mg just begins [23]. In other words, there is a transfer process of deformation in the double phase alloy, so the yield strength is higher compared with that of the single phase alloy. When the Li content continues to increase to 12% and 14%, the matrix of the LAZ*x*32-0.5Y alloys has been completely transformed into β-Li. The strength and hardness of the as-cast LAZ1232-0.5Y and LAZ1432-0.5Y alloys increase substantially while the elongation decreases sharply, which cannot be explained by the matrix alone.

(2) Second phase analysis: AlLi, $MgLi_2Al$ and Al_2Y phases are detected in the as-cast LAZ*x*32-0.5Y alloys (except LAZ432-0.5Y). Among these second phases, AlLi is a softening phase and is not effective in strengthening the alloy [24,25]. $MgLi_2Al$ is a strengthening phase that can significantly enhance the strength of alloy [26,27]. Al_2Y has a face-centered cubic crystal structure with high hardness and melting point. Al_2Y is preferentially formed and acts as heterogeneous nuclei for grains during solidification and hinders the growth of grains, so it has the effect of grain refinement and second phase strengthening [28,29]. It can be seen from Fig. 1 that the content of AlLi and $MgLi_2Al$ gradually increases with increasing Li content, while the content of Al_2Y remains almost constant. The Y content in the LAZ*x*32-0.5Y alloys is fixed (0.5%), and the content of the generated Al_2Y (0.27% to 0.30%) does not differ much among the alloys. Therefore, although Al_2Y has a good strengthening effect, the variation of strength with

Li content is not related to Al_2Y. When the Li content is between 4% and 10%, the mechanical properties are mainly influenced by the matrix. When the Li content is high enough and the matrix is completely transformed into β-Li, the mechanical properties are mainly influenced by the second phase, especially the $MgLi_2Al$ phase. With the increase of Li content, the $MgLi_2Al$ phase gradually increases. These nano-scale $MgLi_2Al$ particles are uniformly distributed in the β-Li matrix, leading to a good diffusion strengthening effect. Therefore, when the Li content increases to 12% and 14%, the yield strength, ultimate tensile strength and hardness of the LAZ*x*32-0.5Y alloys increase significantly, while the elongation decreases sharply.

(3) Solid solution analysis: most of the Al in the as-cast LAZ*x*32-0.5Y alloys forms intermetallic compounds with Li and Y. What's more, these intermetallic compounds gradually increase with the increase of Li content, which leads to the decrease of Al solid dissolved into the matrix. Therefore, the solid solution strengthening effect of Al decreases with the increase of Li content. In other words, the solid solution effect of Al is not beneficial to the strength enhancement of the as-cast LAZ1232-0.5Y and LAZ1432-0.5Y alloys. Zn is mainly solid dissolved in the matrix (especially in the β-Li matrix), which is beneficial for strengthening the β-Li matrix. It has been shown that the solid solution of Zn in Mg alloys is less than 2%(mole fraction) and the solid solution strengthening is almost negligible [30]. The solid solution of Zn in the as-cast LAZ*x*32-0.5Y alloys ranges from 0.68 % to 0.56 %(mole fraction), so the solid solution strengthening effect of Zn is weak and negligible. Y mainly forms the Al_2Y phase, and only a little Y is solid dissolved in the matrix (see Fig. 3). Compared with Zn, Y has a large relative atomic mass and a low solid solubility, so the solid solution strengthening effect of Y is also negligible.

In summary, when the Li content increases from 4% to 10%, the tensile strength and hardness of the as-cast LAZ*x*32-0.5Y alloys gradually decrease, the elongation gradually increases, and the yield strength first increases and then decreases. This is mainly related to the matrix phase transformation of the alloy. When the Li content increases to above 10%, the yield strength, ultimate tensile strength and hardness of the as-cast LAZ*x*32-0.5Y alloy increase continuously with the increase of Li content, while the elongation decreases significantly. The increase of the nano-scale $MgLi_2Al$ phase is the main reason.

With the increase of Li content from 4% to 14%, the fracture mode of the as-cast LAZ*x*32-0.5Y alloys shows an obvious transformation: cleavage fracture → quasi-cleavage fracture → dimple fracture → quasi-cleavage fracture → intergranular fracture. This phenomenon indicates that the ductility of the alloy changes from poor to good and then to poor. When the Li content is 4%, the matrix phase is α-Mg with hcp structure. The slip systems of α-Mg are fewer and hard to deform. Therefore, the fracture is mainly based on cleavage fracture. Cleavage fracture is a brittle fracture mechanism, which is a process of rapid separation along a certain crystallographic plane caused by the breaking of atomic bonds during stretching. With the increase of Li content, softer β-Li matrix appears in the alloy and the content of β-Li matrix increases, resulting in the fracture with both the morphological characteristics of a cleavage fracture (i.e., cleavage steps) and ductile fracture (tearing ridges and dimples). This fracture morphology is between the cleavage fracture and ductile fracture, and its fracture mechanism is quasi-cleavage fracture. When the Li content continues to increase to 10%, the alloy fracture is covered with equiaxed dimples, which is a typical dimple fracture, and the fracture mechanism is microporous aggregation fracture. The micro-pore is formed by the breakage of the second phase itself or the detachment of the interface between the second phase and the matrix. This is also the reason why many second phase particles can be observed at the bottom of the dimples. These micropores gradually grow and form microcracks, which leads to the fracture failure of the alloy. As the Li content continues to increase to 12% and 14%, a large number of second phases are distributed in the matrix and along the grain boundaries. During the tensile deformation, many dislocations accumulate in the second phases and grain boundaries, resulting in excessive stress concentration, so the fracture morphology of the alloy changes from the typical dimples fracture morphology to a quasi-cleavage fracture morphology, and even evolves to intergranular fracture. Intergranular fracture is a typical brittle fracture formed by polycrystals separated from each

other along the grain interfaces, and the main feature is that the fracture surface is icing-like with grain boundary facets.

5 Conclusions

(1) When the Li content increases from 4% to 14%, the matrix of the as-cast LAZ*x*32-0.5Y alloys changes from *α*-Mg single phase to *α*-Mg+*β*-Li double phase and then to *β*-Li single phase. All the alloys contain AlLi and Al_2Y, while $MgLi_2Al$ only appears in the alloy containing *β*-Li. As the Li content increases, the content of AlLi and $MgLi_2Al$ gradually increases, while the content of Al_2Y does not change much. The fine filamentous AlLi phase is distributed in the *α*-Mg matrix in eutectic form, while the granular AlLi phase is distributed in the *β*-Li matrix. The Al_2Y phase is distributed in the matrix and is massive or long strips.

(2) When the Li content increases from 4% to 10%, the ultimate tensile strength and hardness of the as-cast LAZ*x*32-0.5Y alloys gradually decrease, the yield strength first increases and then decreases, and the elongation gradually increases. This is mainly related to the matrix phase transformation of the alloy. When the Li content continues to increase to 10% and 14%, the yield strength, ultimate tensile strength and hardness of the as-cast LAZ*x*32-0.5Y alloys gradually increase and are higher than those of other alloys, while the elongation decreases sharply. This is mainly attributed to the nano-scale $MgLi_2Al$ phase uniformly distributed in the *β*-Li matrix.

(3) When the Li content increases from 4% to 14%, the fracture of the as-cast LAZ*x*32-0.5Y alloys undergoes the following morphological evolution: cleavage steps → cleavage steps + tearing ridges + dimples → dimples → tearing ridges + dimples → icing sugar-like, corresponding to the fracture mechanism: cleavage fracture → quasi-cleavage fracture → microporous aggregation fracture → quasi-cleavagefracture → intergranular fracture. With the increase of Li content, the fracture mode evolves from brittle fracture to ductile fracture and then to brittle fracture, which is consistent with the results of elongation.

Acknowledgments

This study was financially supported by the National Natural Science Foundation of China (Nos. 51821001, U2037601) and Open Fund of State Key Laboratory of Advanced Forming Technology and Equipment (No. SKL2020005).

References

[1] LI C, HE Y, HUANG H. Effect of lithium content on the mechanical and corrosion behaviors of HCP binary Mg−Li alloys [J]. Journal of Magnesium and Alloys, 2021, 9(2): 569−580.

[2] PENG X, LIANG X, LIU W, WU G, JI H, TONG X, ZHANG L, DING W. High-cycle fatigue behavior of Mg−8Li−3Al−2Zn−0.5Y alloy under different states [J]. Journal of Magnesium and Alloys, 2021, 9(5): 1609−1618.

[3] CHANG T C, WANG J Y, CHU C L, LEE S. Mechanical properties and microstructures of various Mg−Li alloys [J]. Materials Letters, 2006, 60(27): 3272−3276.

[4] YU Gang, LIU Yue-long, LI Ying, YE Li-yuan, GUO Xiao-hua, ZHAO Liang. Corrosion and protection of magnesium alloys [J]. The Chinese Journal of Nonferrous Metals, 2002, 12(6): 1087−1098. (in Chinese)

[5] GUO Qing-wei, WANG Gui-sheng, GUO Geng-chen. Binary alloy phase atlas of commonly used non-ferrous metals [M]. Beijing: Chemical Industry Press, 2010. (in Chinese)

[6] ZHAO J, ZHANG J, LIU W, WU G, ZHANG L. Effect of Y content on microstructure and mechanical properties of as-cast Mg−8Li−3Al−2Zn alloy with duplex structure[J]. Materials Science and Engineering A, 2016, 650: 240−247.

[7] FENG S, LIU W, ZHAO J, WU G, ZHANG H, DING W. Effect of extrusion ratio on microstructure and mechanical properties of Mg−8Li−3Al−2Zn−0.5Y alloy with duplex structure [J]. Materials Science and Engineering A, 2017, 692: 9−16.

[8] DOBKOWSKA A, ADAMCZYK-CIEŚLAK B, KUBÁSEK J, VOJTĚCH D, MIZERA J. Microstructure and corrosion resistance of a duplex structured Mg−7.5Li−3Al−1Zn [J]. Journal of Magnesium and Alloys, 2021, 9(2): 467−477.

[9] TANG Y, JIA W, LIU X, LE Q, ZHANG Y. Fabrication of high strength *α*, *α*+*β*, *β* phase containing Mg−Li alloys with 0.2%Y by extruding and annealing process [J]. Materials Science and Engineering A, 2016, 675: 55−64.

[10] LIU W, FENG S, LI Z, ZHAO J, WU G, WANG X, XIAO L, DING W. Effect of rolling strain on microstructure and tensile properties of dual-phase Mg−8Li−3Al−2Zn−0.5Y alloy [J]. Journal of Materials Science & Technology, 2018, 34(12): 2256−2262.

[11] CUI C, WU L, WU R, ZHANG J, ZHANG M. Influence of yttrium on microstructure and mechanical properties of as-cast Mg−5Li−3A−2Zn alloy [J]. Journal of Alloys and Compounds, 2011, 509(37): 9045−9049.

[12] ZHANG Mi-lin, ELKIN F M. Magnesium−lithium ultra-light alloy [M]. Beijing: Science Press, 2010. (in Chinese)

[13] CUI Chong-liang. Effect of rare earth on the microstructure, properties and texture of *α*-Mg−Li alloy [D]. Harbin: Harbin Engineering University, 2013. (in Chinese)

[14] FEI P, QU Z, WU R. Microstructure and hardness of Mg−9Li−6Al−*x*La (*x*=0, 2, 5) alloys during solid solution

treatment [J]. Materials Science and Engineering A, 2015, 625: 169−176.
[15] SUN Y, WANG R, PENG C, WANG X. Microstructure and corrosion behavior of as-homogenized Mg−*x*Li−3Al−2Zn−0.2Zr alloys (*x*=5, 8, 11 wt.%) [J]. Materials Characterization, 2020, 159: 110031.
[16] ZHAN Hai-bo. Study of the ageing behavior of Mg−9Li−*x*Al (=3,6) alloys [D]. Harbin: Harbin Engineering University, 2012. (in Chinese)
[17] XU T C, PENG X D, QIN J, CHEN Y, YANG Y, WEI G. Dynamic recrystallization behavior of Mg−Li−Al−Nd duplex alloy during hot compression [J]. Journal of Alloys and Compounds, 2015, 639: 79−88.
[18] KIM Y H, KIM J H, YU H S, CHOI J W, SON H T. Microstructure and mechanical properties of Mg−*x*Li−3Al−1Sn−0.4 Mn alloys (*x*=5, 8 and 11 wt.%) [J]. Journal of Alloys and Compounds, 2014, 583: 15−20.
[19] LIU B, ZHANG M, WU R. Effects of Nd on microstructure and mechanical properties of as-cast LA141 alloys [J]. Materials Science and Engineering A, 2008, 487(1/2): 347−351.
[20] WANG T, ZHANG M, WU R. Microstructure and properties of Mg−8Li−1Al−1Ce alloy [J]. Materials Letters, 2008, 62(12/13): 1846−1848.
[21] ALAMO A, BANCHIK A D. Precipitation phenomena in the Mg−31at.%Li−1at.%Al alloy [J]. Journal of Materials Science, 1980, 15(1): 222−229.
[22] KANG Z X, LIN K, ZHANG J Y. Characterisation of Mg−Li alloy processed by solution treatment and large strain rolling [J]. Materials Science and Technology, 2016, 32(5): 498−506.
[23] ZOU Yun. Effects of alloying elements and processing on deformation mechanisms and properties of Mg−Li alloys [D]. Harbin: Harbin Engineering University, 2016. (in Chinese)
[24] WU H Y, GAO Z W, LIN J Y, CHIU C H. Effects of minor scandium addition on the properties of Mg−Li−Al−Zn alloy [J]. Journal of Alloys and Compounds, 2009, 474(1/2): 158−163.
[25] GUO X, WU R, ZHANG J, LIU B, ZHANG M. Influences of solid solution parameters on the microstrucuture and hardness of Mg−9Li−6Al and Mg−9Li−6Al−2Y [J]. Materials & Design, 2014, 53: 528−533.
[26] WU S K, LI Y H, CHIEN K T, CHIEN C, YANG C S. X-ray diffraction studies on cold-rolled/solid-solution treated *α*+*β* Mg−10.2Li−1.2Al− 0.4Zn alloy [J]. Journal of Alloys and Compounds, 2013, 563: 234−241.
[27] WU R, ZHANG M. Microstructure, mechanical properties and aging behavior of Mg−5Li−3Al−2Zn−*x*Ag [J]. Materials Science and Engineering A, 2009, 520(1/2): 36−39.
[28] CUI C, WU L, WU R, ZHANG J, ZHANG M. Influence of yttrium on microstructure and mechanical properties of as-cast Mg−5Li−3Al−2Zn alloy [J]. Journal of Alloys and Compounds, 2011, 509(37): 9045−9049.
[29] PENG X, LIU W, WU G, JI H, DING W. Plastic deformation and heat treatment of Mg−Li alloys: A review [J]. Journal of Materials Science and Technology, 2022, 99: 193−206.
[30] HUANG H, YUAN G, CHU Z, DING W. Microstructure and mechanical properties of double continuously extruded Mg−Zn−Gd-based magnesium alloys [J]. Materials Science and Engineering A, 2013, 560: 241−248.

Li 含量对铸态 Mg−*x*Li−3Al−2Zn−0.5Y 合金微观组织与力学性能的影响

彭 翔，刘文才，吴国华

上海交通大学 材料科学与工程学院 轻合金精密成型国家工程中心和金属基复合材料国家重点实验室，上海 200240

摘 要：通过 XRD、SEM、TEM 等微观表征和力学性能测试，研究 Li 含量对铸态 Mg−*x*Li−3Al−2Zn−0.5Y (LAZ*x*32-0.5Y)合金微观组织与力学性能的影响。结果表明：当 Li 含量从 4%增加 14%(质量分数)时，合金的基体相由 *α*-Mg 单相转变为 *α*-Mg+*β*-Li 双相再转变为 *β*-Li 单相。所有合金中都含有 AlLi 相和 Al_2Y 相，而 $MgLi_2Al$ 相只出现在含有 *β*-Li 基体的合金中。随着 Li 含量的增加，AlLi 相和 $MgLi_2Al$ 相的含量逐渐增多，而 Al_2Y 相的含量变化不大。当 Li 含量从 4%增加至 10%时，铸态 LAZ*x*32-0.5Y 合金的抗拉强度和硬度逐渐降低而伸长率逐渐增加，对应的断裂机理由解理断裂转变为准解理断裂再到微孔聚集型断裂，这主要归因于合金中 *α*-Mg 基体逐渐减少而 *β*-Li 基体逐渐增多。当 Li 含量继续增加至 10%和 14%时，铸态 LAZ*x*32-0.5Y 合金的屈服强度、抗拉强度和硬度逐渐增加而伸长率则急剧下降，这主要归因于 *β*-Li 基体中弥散分布的纳米级 $MgLi_2Al$ 相。

关键词：Mg−Li 合金；Li 含量；合金化；微观组织；力学性能

(Edited by Sai-qian YUAN)